Avid lysosomal acidification in fibroblasts of the Mediterranean mouse *Mus spretus*

Melissa Sui[1], Joanne Teh[1], Kayleigh Fort[1], Daniel Shaw[2], Peter Sudmant[3], Tsuyoshi Koide[4], Jeffrey M. Good[2], Juan M. Vazquez*[3], Rachel B. Brem*[1]

Departments of [1]Plant and Microbial Biology and [3]Integrative Biology, University of California, Berkeley, Berkeley, CA 94720, USA

[2]Division of Biological Sciences, University of Montana, Missoula, MT 59812, USA

[4]National Institute of Genetics, Mishima, Shizuoka 411-8540, Japan

*To whom correspondence should be addressed: juan@vazquez.bio, rbrem@berkeley.edu

Abstract

Failures of the lysosome-autophagy system are a hallmark of aging and many disease states. As a consequence, interventions that enhance lysosome function are of keen interest in the context of drug development. Throughout the biomedical literature, evolutionary biologists have discovered that challenges faced by humans in clinical settings have been resolved by non-model organisms adapting to wild environments. Here, we used a primary cell culture approach to survey lysosomal characteristics in selected species of the genus *Mus*. We found that cells from *M. musculus*, mice adapted to human environments, had weak lysosomal acidification and high expression and activity of the lysosomal enzyme β-galactosidase, a classic marker of cellular senescence. Cells of wild relatives, especially the Mediterranean mouse *M. spretus,* had more robustly performing lysosomes and dampened β-galactosidase levels. We propose that classic laboratory models of lysosome function and senescence may reflect characters that diverge from the phenotypes of wild mice. The *M. spretus* phenotype may ultimately provide a blueprint for interventions that ameliorate lysosome breakdown in stress and disease.

Introduction

Many aspects of metazoan health hinge on the ability of the lysosome-autophagy pathway to recycle damaged macromolecules and to direct cell growth decisions (Shin & Zoncu 2020). Indeed, interventions that act broadly to promote health and longevity often require the lysosome-autophagy system (Aman *et al*. 2021; Hansen *et al.* 2018; Bareja *et al*. 2019). More specific mechanisms to boost autophagy are also of potential clinical interest, particularly for treatment of proteinopathies and aging etiologies (Bonam *et al*. 2019; Hansen *et al*. 2018). In practice, whether and how to stimulate proteostasis machinery to advance organismal health remains an open question, and the literature describing such manipulations is in its infancy (Simonsen *et al*. 2008; Pyo *et al*. 2013; Pickford *et al*. 2008; Leiva-Rodríguez *et al*. 2018; Shin *et al*. 2013; Liu *et al.* 2023; Bhuiyan *et al*. 2013).

Cellular senescence is a tumor-suppressive program characterized by cell cycle arrest, resistance to apoptosis, and activation of immune signaling in response to stress (Campisi & d'Adda di Fagagna 2007; Campisi 2005; Hornsby 2002). Though senescence mitigates cellular stress and safeguard health, the accumulation of senescent cells in aged tissues leads to dysfunctional tissue remodeling and chronic inflammation (Krtolica *et al.* 2001; Parrinello *et al.* 2005; Davalos *et al.* 2010; Olivieri *et al.* 2018; Wan *et al.* 2021). In senescent cells, lysosomes increase in size, and lysosomal β-galactosidase becomes active at sub-optimal pH (Robbins *et al.* 1970, Magalhães & Passos 2018, Dodig *et al.* 2019, Curnock *et al.* 2023). Though the exact role of lysosomes in senescence has not been fully elucidated, enhancements to their function have been associated with reduced cellular degeneration and diminished inflammation (Green *et al.* 2011, Carmona-Gutierrez *et al.* 2016, Rovira *et al.* 2022).

Against a backdrop of decades of work in laboratory systems, ecologists have cataloged stress- and disease-resistance traits in wild genotypes from unusual niches, perhaps most famously in

long-lived animal species (Oka *et al*. 2023; Chusyd *et al*. 2021; Finch 2009). Cell-based surveys represent a powerful approach to find and dissect these natural resilience programs. One particularly fruitful discipline has profiled the variation in chemical stress resistance across primary cells from panels of non-model animal species, including, in landmark cases, discovery of the underlying mechanisms (Tian *et al*. 2019; Harper *et al*. 2007; Attaallah *et al*. 2020; Sulak *et al.* 2016). Cellular senescence has also been shown to vary across animal species in *in vitro* models (Attaallah *et al*. 2020; Kang *et al*. 2023; Zhao *et al*. 2018; Gomez *et al.* 2012).

In this study, we aimed to leverage species-specific variation in lysosomal markers of cellular senescence within the *Mus* genus to investigate how evolutionary processes have shaped lysosomal function. Mouse species in this genus shared a common ancestor 7-8 million years ago, and as they radiated across Eurasia, *M. musculus* subspecies came to occupy human-associated niches, whereas other taxa are still found exclusively in the wild (Pagès *et al.* 2015, Smissen & Rowe 2018). Our previous case study (Kang *et al.* 2023) found differences in senescence behaviors, including lysosome markers, across fibroblasts from *M. musculus* subspecies and *M. spretus*, a wild relative that diverged 1-3 million years ago (Morgan *et al*. 2022; Dejager *et al*. 2009). Here, we aimed to build on these observations to gain a deeper understanding of lysosomal programs in non-model mice, focusing on the contrasts between the genotypes of human commensal and laboratory mice and those of their wild relatives.

Results

M. spretus fibroblasts exhibit reduced lysosomal β-galactosidase activity

To extend our initial observation of divergent cellular senescence behaviors across *Mus* (Kang *et al.* 2023), we established a panel of primary tail skin fibroblasts from four wild-derived strains of *M. m. musculus* (PWK/PhJ, BLG2/Ms, CHD/Ms, MSM/Ms), two wild-derived strains of *M. m. domesticus* (ManB/NachJ, TUCA/NachJ), an admixed classic laboratory strain of mostly *M. m. domesticus* origin (C57BL/6J), a wild-derived strain of the steppe mouse *M. spicilegus* (ZRU), and two wild-derived strains of the Mediterranean mouse *M. spretus* (STF/Pas, SFM/Pas). We subjected each culture to 15 Gy of infrared irradiation and incubated for 10 days, which is sufficient to induce DNA damage response, arrested cell growth, and senescence expression programs in fibroblasts from across the genus (Kang *et al*. 2023). We first assayed each culture for lysosomal β-galactosidase, as a standard marker of senescence that reports exhaustion of protein quality control in the lysosome (Campisi & d'Adda di Fagagna 2007; Kang *et al*. 2023; Casella *et al*. 2019; Guerrero-Navarro *et al*. 2022; Carmona-Gutierrez *et al*. 2016). Fibroblasts of each genotype displayed the anticipated increase in β-galactosidase activity following irradiation, compared to their respective control counterparts (Figure 1B). Whereas cells from strains of each species behaved similarly, we observed significant differences between species: irradiated *M. spretus* fibroblasts exhibited β-galactosidase signal ~2-fold lower than did cells from *M. m. musculus* and *M. m. domesticus,* and staining of *M. spicilegus* cells was between the two extremes (Figure 1B). To follow up on this difference, we used an alternative approach for senescence induction with the radiomimetic drug neocarzinostatin, which induces senescence in mouse cells at 3.6 μM (Ito *et al.* 2018, Correia□Melo *et al.* 2016). Fibroblasts treated with

neocarzinostatin exhibited a pattern mimicking that we had seen under radiation, with the treatment inducing elevated β-galactosidase activity in all cultures, and cells from *M. spretus* staining lower than those of sister taxa (Figure 1C). Furthermore, the same trend was detectable in cells cultured in the absence of DNA damage: fibroblasts from *M. musculus* subspecies exhibited higher β-galactosidase staining than those of *M. spicilegus*, which stained higher than *M. spretus*. The latter species differences from untreated cells were of smaller magnitude than those manifesting after stress, and this dependence on treatment was statistically significant (Figures 1 and S1). Thus, *M. spretus* fibroblasts exhibited dampened β-galactosidase activity relative to other genotypes, with amplification of the effect under stress. Controls ruled out culture passage number as a driver of the variation (Figure S2).

In principle, differences in the senescence-apoptosis fate choice after DNA damage (Childs *et al.* 2014; Zhao *et al*. 2018; Attaallah *et al*. 2020) could contribute to the divergence between mouse genotypes that we had seen in fibroblast β-galactosidase staining. To explore this, we measured Caspase 3/5 activity in fibroblasts in response to irradiation (Figure S3A) and neocarzinostatin treatment (Figure S3B). The results showed no consistent patterns of apoptosis either within or between species' genotypes, arguing against a role for apoptosis activation in species differences in fibroblast β-galactosidase activity.

To establish further the robustness of *Mus* species differences in fibroblast β-galactosidase activity, we considered the dose-response relationship with stress. We compared primary fibroblasts from *M. m. musculus* PWK and *M. spretus* STF as representatives of their respective species, in each case assaying β-galactosidase upon irradiation at increasing doses. The results revealed a consistent ~2-fold difference between the genotypes at each dose (Figure S4), a magnitude slightly exceeding the species divergence in the untreated control, consistent with our survey across genotypes at fixed stress doses (Figure 1). These data ruled out a switch by *M. spretus* fibroblasts into a high-amplitude, *M. musculus*-like program above a certain threshold of stress exposure. We conclude instead that *M. spretus* cells are hard-wired for lower β-galactosidase activity in all tested conditions—including the resting state.

No consistent divergence in senescence signaling across *Mus* species fibroblasts

We reasoned that the differences in β-galactosidase activity in fibroblasts among the *Mus* species we tested were likely mediated by mechanisms unrelated to senescence itself. As a first investigation of this idea, we explored senescence signaling, using as a readout P21, a regulator of immune recruitment and cell cycle arrest in senescence (Gu *et al*. 2013; Yew *et al*. 2011). We quantified levels of P21 protein in response to either irradiation or neocarzinostatin, with fibroblasts from *M. m. musculus* PWK and *M. spretus* STF as a testbed. Results showed the expected induction of P21 in fibroblasts from both species in response to irradiation or neocarzinostatin (Figure S5). In investigating quantitative patterns among these P21 induction behaviors, we noted some species-specific differences, though they were not of consistent direction: *M. spretus* cells induced P21 protein abundance more than did *M. musculus* under neocarzinostatin treatment but less following irradiation and in untreated controls (Figure S5). These changes could reflect the differential activity of alternate senescence signaling pathways

(Saul *et al*. 2023) between species in some treatments. However, given our focus on lysosomal β-galactosidase differences between *M. musculus* and *M. spretus* across all tested conditions (Figure 1), we concluded that P21 regulation was not a consistent correlate of this phenotype and not a compelling candidate for its underlying mechanism. Indeed, in analysis of mRNA expression profiles (Kang *et al.* 2023), we detected no differences in induction of the P21 gene (*CDKN1A*) between *M. musculus* and *M. spretus* fibroblasts in response to stress (Figure S6).

M. spretus fibroblasts exhibit strongly acidified lysosomes

To advance our search to understand *Mus* species differences in β-galactosidase activity in the fibroblast model, we next focused on regulation of the enzyme itself. Transcriptional profiling data from fibroblasts revealed 1.5 to 2-fold higher expression of the lysosomal β-galactosidase *GLB1* in *M. musculus* fibroblasts than in those of *M. spretus*, regardless of treatment (Figure S7A). Allele-specific expression measurements in stressed and control fibroblasts from an interspecies F1 hybrid made clear that this change was regulated in *cis*: that is, the *M. musculus* allele of *GLB1* drove higher expression of its own encoding locus than the *M. spretus* allele, when both were in the same nucleus (Figure S7B). Thus, the species changes in β-galactosidase activity we had noted in terms of cell biology in fibroblasts (Figure 1) were mirrored by regulation of gene expression, including robust differences between genotypes in unstressed control conditions.

We hypothesized that the higher β-galactosidase expression and activity we had seen in *M. musculus* fibroblasts could be a consequence of heightened need owing to failures elsewhere in the proteostasis system, relative to cells of *M. spretus*. To explore this, we assayed lysosomal acidity with the Lysotracker stain, again making use of *M. m. musculus* PWK and *M. spretus* STF as a test system. Conforming to our prediction, *M. spretus* cells exhibited 3-fold stronger Lysotracker signal relative to cells of *M. musculus,* in untreated cultures (Figure 2, left). The species difference persisted in cultures induced to senesce with irradiation (Figure 2, middle) and neocarzinostatin (Figure 2, right). Taken together, our results establish a trait syndrome of elevated lysosomal acidification and low β-galactosidase expression and activity in *M. spretus* fibroblasts relative to those of other mice, whether the cells are senescent or not.

Discussion

For decades, biomedical researchers have relied on strains from the *M. musculus* clade as the standard for studying lysosomal and senescence biology. In this work, we have demonstrated that lysosomal phenotypes vary quantitatively across *Mus* in fibroblast culture models, and that in contrast to *M. musculus*, cells from the non-commensal mouse *M. spretus* exhibit a lysosomal acidity and β-galactosidase program of the kind that, in the experimental literature, has been associated with healthy aging and disease resistance.

When experimentally induced in laboratory cell models, a backup in the lysosomal-autophagy system triggers compensatory increases in lysosomal mass and number, for which high β-galactosidase activity is a robust marker (Curnock *et al.* 2023; Delfarah *et al*. 2021; Lee *et al*.

2006, Dimri *et al.* 1995, Rovira *et al.* 2022). We propose a similar causal relationship between the two phenotypes we have observed as they vary across *Mus* fibroblasts. Under this model, the elevated β-galactosidase expression and activity in *M. musculus* cells would represent compensation for their weak lysosomal acidification in comparison to *M. spretus* genotypes, even in the absence of experimental stress. The *M. musculus cis*-regulatory allele upregulating β-galactosidase that we have noted in fibroblasts could well represent a genetically encoded component of such a program, a constitutive boost in protein degradation capacity by a regulatory mechanism, in the face of lysosomal acidification defects.

Our work leaves open the question of whether weak lysosomal acidity and high β-galactosidase in fibroblasts represent a state ancestral to *Mus* that was resolved in the *M. spicilegus-M. spretus* lineage, or an evolutionary novelty that arose with commensalism in *M. musculus*. In either case, the evidence that we have seen for conservation across *M. musculus* strains and subspecies strongly suggests a history of constraint in this lineage. If the lysosomal behaviors we have studied here prove to have evolved under selection, they could conceivably relate to body size, response to immune challenges, or association with human ecology as they differ between *M. musculus* and *M. spretus* (Dejager *et al.* 2009, Mahieu *et al.* 2006, Kawakami & Yamamura 2008, Staelens *et al.* 2002, Blanchet *et al.* 2010, Pérez del Villar *et al.* 2013, Harr *et al.* 2016).

Ultimately, as its mechanism is revealed, the high-acidification phenotype of *M. spretus* fibroblasts may prove to be well suited for the development of mimetics that would boost lysosomal function in a human clinical setting. More broadly, our results provide a way forward for the use of wild mouse species as models for lysosomal function and senescence, without the peculiarities of commensal lineages.

Methods

Primary tail fibroblasts were extracted as described by Khan and Gasser (2016). Subsequent culture and experiments used complete medium (DMEM, 10% FBS, 1% pen-strep) in T25 flasks at 37˚C, 3% O_2, and 10% CO_2. Cells were passaged based on confluence using trypsin. Experimental treatments included 15 GY of ionizing irradiation or 3.6 µM neocarzinostatin. Analysis kits used were the Abcam Ltd. Senescence Detection Kit (Cat. #ab65351), ApoTox-Glo™ Triplex Assay (Promega Cat. #G6321), and LysoTracker™ Green DND-26 (Thermo Fisher Cat. #L7526). Primary and secondary antibodies used in western blots were the rabbit monoclonal Anti-p21 antibody (ab188224, Abcam, 1:1000), mouse monoclonal anti-β-tubulin (T9026, Sigma-Aldrich, 1:1000), Goat Anti-Mouse IgG(H+L) Human ads-HRP (Cat#1031-05, Southern Biotech, 1:5000), and Goat Anti-Rabbit IgG(H+L) Human ads-HRP (Cat#4050-05, Southern Biotech, 1:5000). Additional details of methods available in Supplementary Materials.

Acknowledgements

The authors thank Vera Gorbunova, Emilie Tu, Helen Bateup, Samantha Jackson, Linda Wilbrecht, Polly Campbell, and Michael Nachman for animal material; Diana Bautista, Britt Glaunsinger, José Pablo Vázquez-Medina, and Mary West for their generosity with space and resources; Juliana Valencia Lesmes, Mara Baylis, Sam Rider and Harriet Song for technical contributions; and members of the Brem lab for helpful discussions. This work was supported by National Institutes of Health R01NS116992 to RBB and R01GM120430 to RBB and JMG. JMV was supported by the National Science Foundation Postdoctoral Research Fellowship in Biology (#2109915) and by the National Institute for Health T32AG000266 and 1K99AG088361.

Figure captions

Figure 1. Low β-galactosidase activity in *M. spretus* fibroblasts regardless of treatment. In a given panel, each bar length displays the mean percentage of primary fibroblasts of the indicated strain and species that stained positive after administration of the colorimetric β-galactosidase substrate X-Gal. From top to bottom, complete names of the strains are as follows: *M. m. musculus* (PWK/PhJ, BLG2/Ms, CHD/Ms, MSM/Ms), laboratory strain of mostly *M. m. domesticus* origin (C57BL/6J), *M. m. domesticus* (TUCA/NachJ, ManB/NachJ), *M. spicilegus*, and *M. spretus* (SFM, STF/Pas). Panels report results from (A) untreated cells, (B) cells treated with infrared irradiation followed by a 10-day incubation, or (C) cells after 1 hour of neocarzinostatin treatment followed by 24 hours of incubation. Points report biological and technical replicates collected over at least two separate days. Error bars report one standard error above and below the mean. ***, two-tailed Wilcoxon $p < 10\text{-}7$ comparing *M. spretus* with all other genotypes; *M. spretus* and *M. spicilegus* also differed in each panel (Wilcoxon $p < 0.05$). For (B) and (C), in a comparison between the respective treatment and the untreated control in (A), a two-factor ANOVA with treatment and genotype as factors yielded $p < 2e^{-16}$ for the interaction between the two factors.

Figure 2. High lysosomal acidity in *M. spretus* cells across all treatments. Shown are results from assays of the lysosomal acidity reporter Lysotracker on primary fibroblasts of the indicated genotype (*M. spretus,* strain STF; *M. m. musculus*, strain PWK). The y-axis reports mean fluorescence of the indicated culture normalized to the control *M. musculus* sample for each experiment. Pairs of bars report results from untreated cells (left), or cells treated with irradiation followed by a 10-day incubation (middle) or after 1 hour of neocarzinostatin treatment followed by 24 hours of incubation (right). Data points correspond to biological and technical replicates collected over at least two different days, and the bar height reports their mean. Error bars report one standard error above and below the mean. *, Wilcoxon $p < 0.05$, **, Wilcoxon $p < 0.01$.

Supplementary figure captions

Figure S1. Low normalized β-galactosidase activity in *M. spretus* fibroblasts.
Data are as in Figure 1 of the main text, except that measurements from the culture of a given genotype and DNA damage treatment were normalized to the average of all measurements from untreated controls of that genotype. ***, two-tailed Wilcoxon $p < .001$ comparing *M. spretus* with all other genotypes for both treatments.

Figure S2. Fibroblast passage number has no detectable effect on X-Gal staining.
In a given panel, each row reports results from assays of the β-galactosidase substrate X-Gal on fibroblasts of the indicated genotype shown in Figure 1 of the main text, and each point reports one replicate culture. The x-axis reports the passage number of the respective culture and the y-axis reports X-Gal staining. (A) Cells induced to senesce with irradiation (right) and their paired controls (left). (B) Cells induced to senesce with neocarzinostatin (right) and their paired controls (left).

Figure S3. No consistent variation between *Mus* species fibroblasts in apoptosis activity.
Data are as in Figure 1 of the main text, except that for a given genotype and treatment, the x-axis reports caspase activity of the culture measured with the Apotox-Glo assay, normalized to the average from untreated cultures of the respective genotype for each experiment. (A) Outliers trimmed for visualization. (B) Full data set view.

Figure S4. Dose dependence of β-galactosidase staining in *Mus* fibroblasts.
Each trace shows results from assays of the β-galactosidase substrate X-Gal on primary fibroblasts of the indicated genotype (*M. spretus*, strain STF; *M. m. musculus*, strain PWK). For a given trace, the x-axis reports irradiation dosage (in centigray, cGy) at 0 (Control), 1000, 1500, 2000, and 2500 cGy, and the y-axis reports the percentage of X-Gal positive cells in untreated controls or in irradiated cells after 10 days of incubation. Smaller points represent biological and technical replicates, and larger points indicate their mean values. ***, two-factor ANOVA with dosage and species as factors yielded $p < 2e^{-16}$ for each factor.

Figure S5. No consistent variation between *Mus* fibroblasts in P21 abundance.
Shown are results of Western blot assays of abundance of the senescence regulator P21 in primary fibroblasts of the indicated genotype (*M. spretus*, strain STF; *M. m. musculus*, strain PWK). (A) Top, representative blot showing tubulin (55 kDa) and P21 (21 kDa) levels in 25 µg of whole cell lysate (WCL) from untreated control cells or those irradiated (Xray) and incubated for 10 days to establish senescence. Bottom, blot as at top except that cells were treated with 1 hour of neocarzinostatin (NCS) and incubated for 24 hours to establish senescence. (B) Each column reports quantification of P21 protein abundance normalized to tubulin for the indicated genotype and treatment. Data points correspond to biological and technical replicates collected over at least two different days, and the bar height reports their mean. Error bars report one standard error above and below the mean. No comparisons were significant in pairwise Wilcoxon tests. *, two-factor ANOVA with condition and species as factors yielded $p < 0.05$ for species.

Figure S6. No significant variation between *Mus* fibroblasts in Cdkn1a mRNA expression. (A) Shown are measurements of mRNA expression of the β-galactosidase gene Cdkn1a, from profiling of fibroblasts of the indicated genotype (*M. spretus*, strain STF; *M. m. musculus*, strain PWK), untreated or treated with irradiation followed by a 10-day incubation (Kang *et al.* 2023). Data points within each column represent biological and technical replicates and the bar height reports their mean. Error bars report one standard error above and below the mean. Only condition had a significant impact on expression in a two-factor ANOVA with treatment and genotype as factors ($p < 0.005$, **).

Figure S7. Variation between *Mus* fibroblasts in Glb1 mRNA expression. (A) Shown are measurements of mRNA expression of the β-galactosidase gene from profiling of fibroblasts of the indicated genotype (*M. spretus*, strain STF; *M. m. musculus*, strain PWK), untreated or treated with irradiation followed by a 10-day incubation (Kang *et al.* 2023). Data points within each column represent biological and technical replicates and the bar height reports their mean. Only the effect of genotype was significant in a two-factor ANOVA with condition and species as factors (*, $p < 0.05$). (B) Data are as in (A), except that allele-specific mRNA expression of the β-galactosidase gene was measured from profiling of fibroblasts of an F1 hybrid between STF and PWK. (*M. spretus*, strain STF; *M. m. musculus*, strain PWK)(Kang *et al.* 2023). In a two-factor ANOVA with condition and genotype as factors, both had significant effects (species $p < 0.0005$, ***; condition $p < 0.05$, *).

References

Admasu TD, Rae MJ & Stolzing A (2021) Dissecting primary and secondary senescence to enable new senotherapeutic strategies. *Ageing Research Reviews* 70, 101412.

Aman Y, Schmauck-Medina T, Hansen M, Morimoto RI, Simon AK, Bjedov I, Palikaras K, Simonsen A, Johansen T, Tavernarakis N, Rubinsztein DC, Partridge L, Kroemer G, Labbadia J & Fang EF (2021) Autophagy in healthy aging and disease. *Nat Aging* 1, 634–650.

Attaallah A, Lenzi M, Marchionni S, Bincoletto G, Cocchi V, Croco E, Hrelia P, Hrelia S, Sell C & Lorenzini A (2020) A pro longevity role for cellular senescence. *Geroscience* 42, 867–879.

Bareja A, Lee DE & White JP (2019) Maximizing Longevity and Healthspan: Multiple Approaches All Converging on Autophagy. *Front Cell Dev Biol* 7, 183.

Bhuiyan MS, Pattison JS, Osinska H, James J, Gulick J, McLendon PM, Hill JA, Sadoshima J & Robbins J (2013) Enhanced autophagy ameliorates cardiac proteinopathy. *J Clin Invest* 123, 5284–5297.

Blanchet C, Jaubert J, Carniel E, Fayolle C, Milon G, Szatanik M, Panthier J-J & X Montagutelli (2011) Mus spretus SEG/Pas mice resist virulent Yersinia pestis, under multigenic control. *Genes Immun* 12, 23–30.

Bonam SR, Wang F & Muller S (2019) Lysosomes as a therapeutic target. *Nat Rev Drug Discov* 18, 923–948.

Campisi J (2005) Senescent cells, tumor suppression, and organismal aging: good citizens, bad neighbors. *Cell* 120, 513–522.

Campisi J & d'Adda di Fagagna F (2007) Cellular senescence: when bad things happen to good cells. *Nat Rev Mol Cell Biol* 8, 729–740.

Carmona-Gutierrez D, Hughes AL, Madeo F & Ruckenstuhl C (2016) The crucial impact of lysosomes in aging and longevity. *Ageing Res Rev* 32, 2–12.

Casella G, Munk R, Kim KM, Piao Y, De S, Abdelmohsen K & Gorospe M (2019) Transcriptome signature of cellular senescence. *Nucleic Acids Res* 47, 7294–7305.

Childs BG, Baker DJ, Kirkland JL, Campisi J & van Deursen JM (2014) Senescence and apoptosis: dueling or complementary cell fates? *EMBO Rep* 15, 1139–1153.

Chusyd DE, Ackermans NL, Austad SN, Hof PR, Mielke MM, Sherwood CC & Allison DB (2021) Aging: What We Can Learn From Elephants. *Front Aging* 2, 726714.

Correia□Melo C, Marques FD, Anderson R, Hewitt G, Hewitt R, Cole J, Carroll BM, Miwa S, Birch J, Merz A, Rushton MD, Charles M, Jurk D, Tait SW, Czapiewski R, Greaves L, Nelson G, Bohlooly-Y M, Rodriguez-Cuenca S, Vidal-Puig A, Mann D, Saretzki G, Quarato G, Green DR, Adams PD, Von Zglinicki T, Korolchuk VI & Passos JF (2016) Mitochondria are required for pro-ageing features of the senescent phenotype. *The EMBO Journal* 35, 724–742.

Curnock R, Yalci K, Palmfeldt J, Jäättelä M, Liu B & Carroll B (2023) TFEB□dependent lysosome biogenesis is required for senescence. *EMBO J* 42, e111241.

De Magalhães JP & Passos JF (2018) Stress, cell senescence and organismal ageing. *Mechanisms of Ageing and Development* 170, 2–9.

Del Villar LP, Vicente B, Galindo-Villardón P, Castellanos A, Pérez-Losada J & Muro A (2013) Schistosoma mansoni experimental infection in Mus spretus (SPRET/EiJ strain) mice. *Parasite*, 20, 27.

Dejager L, Libert C & Montagutelli X (2009) Thirty years of Mus spretus: a promising future. *Trends Genet* 25, 234–241.

Delfarah A, Hartel NG, Zheng D, Yang J & Graham NA (2021) Identification of a Proteomic Signature of Senescence in Primary Human Mammary Epithelial Cells. *J Proteome Res* 20, 5169–5179.

Dodig S, Čepelak I & Pavić I (2019) Hallmarks of senescence and aging. *Biochem Med (Zagreb)* 29, 030501.

Finch CE (2009) Update on slow aging and negligible senescence--a mini-review. *Gerontology* 55, 307–313.

Gomes NMV, Ryder OA, Houck ML, Charter SJ, Walker W, Forsyth NR, Austad SN, Venditti C, Pagel M, Shay JW & Wright WE (2011) Comparative biology of mammalian telomeres: hypotheses on ancestral states and the roles of telomeres in longevity determination. *Aging Cell* 10, 761–768.

Green DR, Galluzzi L & Kroemer G (2011) Mitochondria and the autophagy-inflammation-cell death axis in organismal aging. *Science* 333, 1109–1112.

456 Gu Z, Jiang J, Tan W, Xia Y, Cao H, Meng Y, Da Z, Liu H & Cheng C (2013) p53/p21
457 Pathway involved in mediating cellular senescence of bone marrow-derived
458 mesenchymal stem cells from systemic lupus erythematosus patients. *Clin Dev*
459 *Immunol* 2013, 134243.

460 Guerrero-Navarro L, Jansen-Dürr P & Cavinato M (2022) Age-Related Lysosomal
461 Dysfunctions. *Cells* 11, 1977.

462 Hansen M, Rubinsztein DC & Walker DW (2018) Autophagy as a promoter of longevity:
463 insights from model organisms. *Nat Rev Mol Cell Biol* 19, 579–593.

464 Harper JM, Salmon AB, Leiser SF, Galecki AT & Miller RA (2007) Skin-derived fibroblasts
465 from long-lived species are resistant to some, but not all, lethal stresses and to the
466 mitochondrial inhibitor rotenone. *Aging Cell* 6, 1–13.

467 Harr B, Karakoc E, Neme R, Teschke M, Pfeifle C, Pezer Ž, Babiker H, Linnenbrink M,
468 Montero I, Scavetta R, Abai MR, Molins MP, Schlegel M, Ulrich RG, Altmüller J,
469 Franitza M, Büntge A, Künzel S & Tautz D (2016) Genomic resources for wild
470 populations of the house mouse, Mus musculus and its close relative Mus spretus. *Sci*
471 *Data* 3, 160075.

472 Hernandez-Segura A, Brandenburg S & Demaria M (2018) Induction and Validation of
473 Cellular Senescence in Primary Human Cells. *J Vis Exp*, 57782.

474 Hooper JM, Rainer E & Banks RA (1996) Haemodialysis patients' knowledge and beliefs
475 about medication. *EDTNA ERCA J* 22, 38–40.

476 Hornsby PJ (2002) Cellular senescence and tissue aging in vivo. *J Gerontol A Biol Sci Med*
477 *Sci* 57, B251-256.

478 Imai Y, Tanave A, Matsuyama M & Koide T (2022) Efficient genome editing in wild strains
479 of mice using the i-GONAD method. *Sci Rep* 12, 13821.

480 Ito T, Teo YV, Evans SA, Neretti N & Sedivy JM (2018) Regulation of Cellular Senescence
481 by Polycomb Chromatin Modifiers through Distinct DNA Damage-and Histone
482 Methylation-Dependent Pathways. *Cell Rep* 22, 3480–3492.

483 Kang T, Moore EC, Kopania EEK, King CD, Schilling B, Campisi J, Good JM & Brem RB
484 (2023) A natural variation-based screen in mouse cells reveals USF2 as a regulator of
485 the DNA damage response and cellular senescence. *G3 (Bethesda)* 13, jkad091.

Kawakami M & Yamamura K-I (2008) Cranial bone morphometric study among mouse strains. *BMC Evolutionary Biology*, 8 (1), 73.

Kirschner K, Rattanavirotkul N, Quince MF & Chandra T (2020) Functional heterogeneity in senescence. *Biochemical Society Transactions* 48, 765–773.

Kreis N-N, Friemel A, Zimmer B, Roth S, Rieger MA, Rolle U, Louwen F & Yuan J (2016) Mitotic p21Cip1/CDKN1A is regulated by cyclin-dependent kinase 1 phosphorylation. *Oncotarget* 7, 50215–50228.

Lee BY, Han JA, Im JS, Morrone A, Johung K, Goodwin EC, Kleijer WJ, DiMaio D & Hwang ES (2006) Senescence-associated beta-galactosidase is lysosomal beta-galactosidase. *Aging Cell* 5, 187–195.

Leiva-Rodríguez T, Romeo-Guitart D, Marmolejo-Martínez-Artesero S, Herrando-Grabulosa M, Bosch A, Forés J & Casas C (2018) ATG5 overexpression is neuroprotective and attenuates cytoskeletal and vesicle-trafficking alterations in axotomized motoneurons. *Cell Death Dis* 9, 626.

Liu X, Ye Q, Huang Z, Li X, Zhang L, Liu X, Wu Y-C, Brockmeier U, Hermann DM, Wang Y-C & Ren L (2023) BAG3 Overexpression Attenuates Ischemic Stroke Injury by Activating Autophagy and Inhibiting Apoptosis. *Stroke* 54, 2114–2125.

Mahieu T, Park JM, Revets H, Pasche B, Lengeling A, Staelens J, Wullaert A, Vanlaere I, Hochepied T, Van Roy F, Karin M, Libert C (2006) The wild-derived inbred mouse strain SPRET/Ei is resistant to LPS and defective in IFN-β production. *Proceedings of the National Academy of Sciences* 103 (7), 2292–2297.

Morgan AP, Hughes JJ, Didion JP, Jolley WJ, Campbell KJ, Threadgill DW, Bonhomme F, Searle JB & de Villena FP-M (2022) Population structure and inbreeding in wild house mice (Mus musculus) at different geographic scales. *Heredity (Edinb)* 129, 183–194.

Mylonas A & O'Loghlen A (2022) Cellular Senescence and Ageing: Mechanisms and Interventions. *Front Aging* 3, 866718.

Oka K, Yamakawa M, Kawamura Y, Kutsukake N & Miura K (2023) The Naked Mole-Rat as a Model for Healthy Aging. *Annu Rev Anim Biosci* 11, 207–226.

Pagès M, Fabre P, Chaval Y, Mortelliti A, Nicolas V, Wells K, Michaux JR & Lazzari V (2015) Molecular phylogeny of South-East Asian arboreal murine rodents. *Zoologica Scripta* 45 (4), 349–364.

Pickford F, Masliah E, Britschgi M, Lucin K, Narasimhan R, Jaeger PA, Small S, Spencer B, Rockenstein E, Levine B & Wyss-Coray T (2008) The autophagy-related protein beclin 1 shows reduced expression in early Alzheimer disease and regulates amyloid beta accumulation in mice. *J Clin Invest* 118, 2190–2199.

Pyo J-O, Yoo S-M, Ahn H-H, Nah J, Hong S-H, Kam T-I, Jung S & Jung Y-K (2013) Overexpression of Atg5 in mice activates autophagy and extends lifespan. *Nat Commun* 4, 2300.

Romanov VS & Rudolph KL (2016) p21 shapes cancer evolution. *Nat Cell Biol* 18, 722–724.

Rovira M, Sereda R, Pladevall-Morera D, Ramponi V, Marin I, Maus M, Madrigal-Matute J, Díaz A, García F, Muñoz J, Cuervo AM & Serrano M (2022) The lysosomal proteome of senescent cells contributes to the senescence secretome. *Aging Cell* 21, e13707.

Shin HR & Zoncu R (2020) The Lysosome at the Intersection of Cellular Growth and Destruction. *Dev Cell* 54, 226–238.

Shin JY, Hong S-H, Kang B, Minai-Tehrani A & Cho M-H (2013) Overexpression of beclin1 induced autophagy and apoptosis in lungs of K-rasLA1 mice. *Lung Cancer* 81, 362–370.

Simonsen A, Cumming RC, Brech A, Isakson P, Schubert DR & Finley KD (2008) Promoting basal levels of autophagy in the nervous system enhances longevity and oxidant resistance in adult Drosophila. *Autophagy* 4, 176–184.

Smissen PJ & Rowe KC (2018) Repeated biome transitions in the evolution of Australian rodents. *Molecular Phylogenetics and Evolution* 128, 182–191.

Staelens J, Wielockx B, Puimège L, Van Roy F, Guénet J-L & Libert C (2002) Hyporesponsiveness of SPRET/Ei mice to lethal shock induced by tumor necrosis factor and implications for a TNF-based antitumor therapy. *Proceedings of the National Academy of Sciences*, 99 (14), 9340–9345.

Sulak M, Fong L, Mika K, Chigurupati S, Yon L, Mongan NP, Emes RD & Lynch VJ (2016) TP53 copy number expansion is associated with the evolution of increased body size and an enhanced DNA damage response in elephants. *eLife* 5, e11994.

Takasugi M, Yoshida Y, Hara E & Ohtani N (2023) The role of cellular senescence and SASP in tumour microenvironment. *The FEBS Journal* 290, 1348–1361.

548 Tian X, Firsanov D, Zhang Z, Cheng Y, Luo L, Tombline G, Tan R, Simon M, Henderson S,
549 Steffan J, Goldfarb A, Tam J, Zheng K, Cornwell A, Johnson A, Yang J-N, Mao Z,
550 Manta B, Dang W, Zhang Z, Vijg J, Wolfe A, Moody K, Kennedy BK, Bohmann D,
551 Gladyshev VN, Seluanov A & Gorbunova V (2019) SIRT6 Is Responsible for More
552 Efficient DNA Double-Strand Break Repair in Long-Lived Species. *Cell* 177, 622-
553 638.e22.

554 Yan J, Chen S, Yi Z, Zhao R, Zhu J, Ding S & Wu J (2024) The role of p21 in cellular
555 senescence and aging-related diseases. *Molecules and Cells* 47, 100113.

556 Yew T-L, Chiu F-Y, Tsai C-C, Chen H-L, Lee W-P, Chen Y-J, Chang M-C & Hung S-C
557 (2011) Knockdown of p21(Cip1/Waf1) enhances proliferation, the expression of
558 stemness markers, and osteogenic potential in human mesenchymal stem cells. *Aging*
559 *Cell* 10, 349–361.

560 Zhao Y, Tyshkovskiy A, Muñoz-Espín D, Tian X, Serrano M, de Magalhaes JP, Nevo E,
561 Gladyshev VN, Seluanov A & Gorbunova V (2018) Naked mole rats can undergo
562 developmental, oncogene-induced and DNA damage-induced cellular senescence.
563 *Proc Natl Acad Sci U S A* 115, 1801–1806.

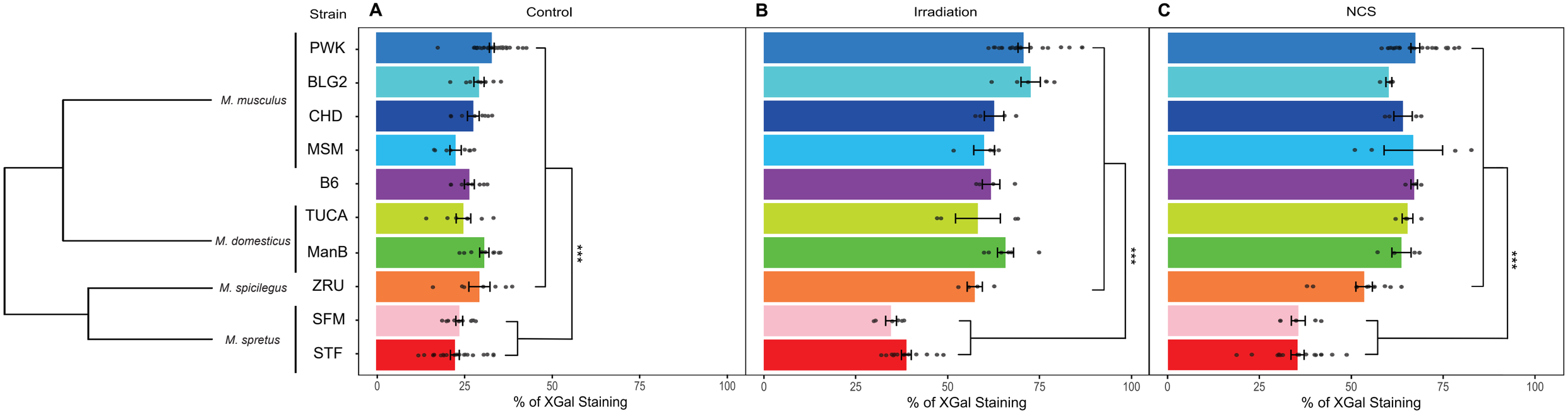
Strain
A
Control
B
Irradiation
C
NCS
PWK
BLG2
CHD
MSM
B6
TUCA
ManB
ZRU
SFM
STF
M. musculus
M. domesticus
M. spicilegus
M. spretus
***
0
25
50
75
100
% of XGal Staining

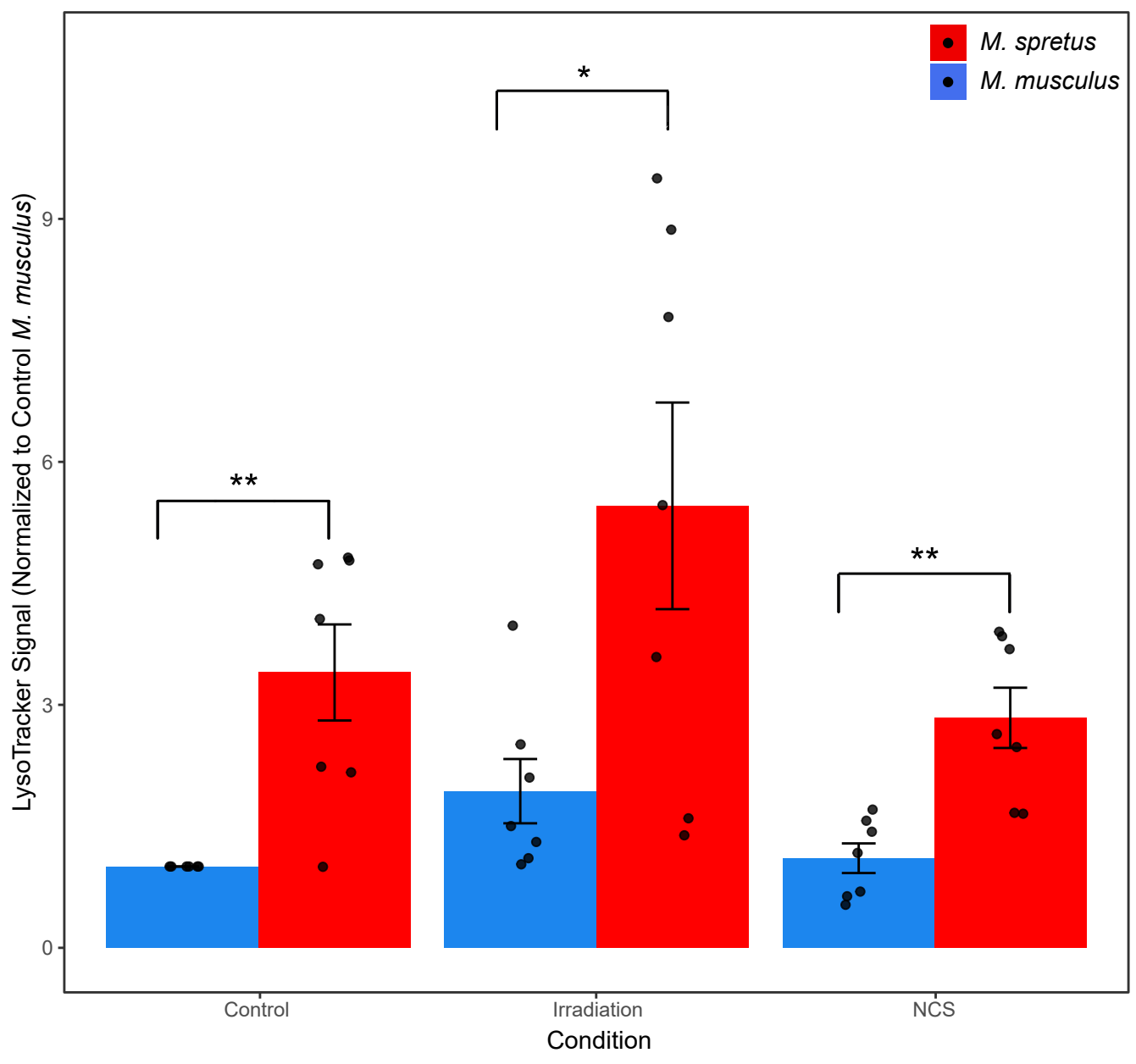
M. spretus
M. musculus
LysoTracker Signal (Normalized to Control M. musculus)
0
3
6
9
*
**
**
Control
Irradiation
NCS
Condition

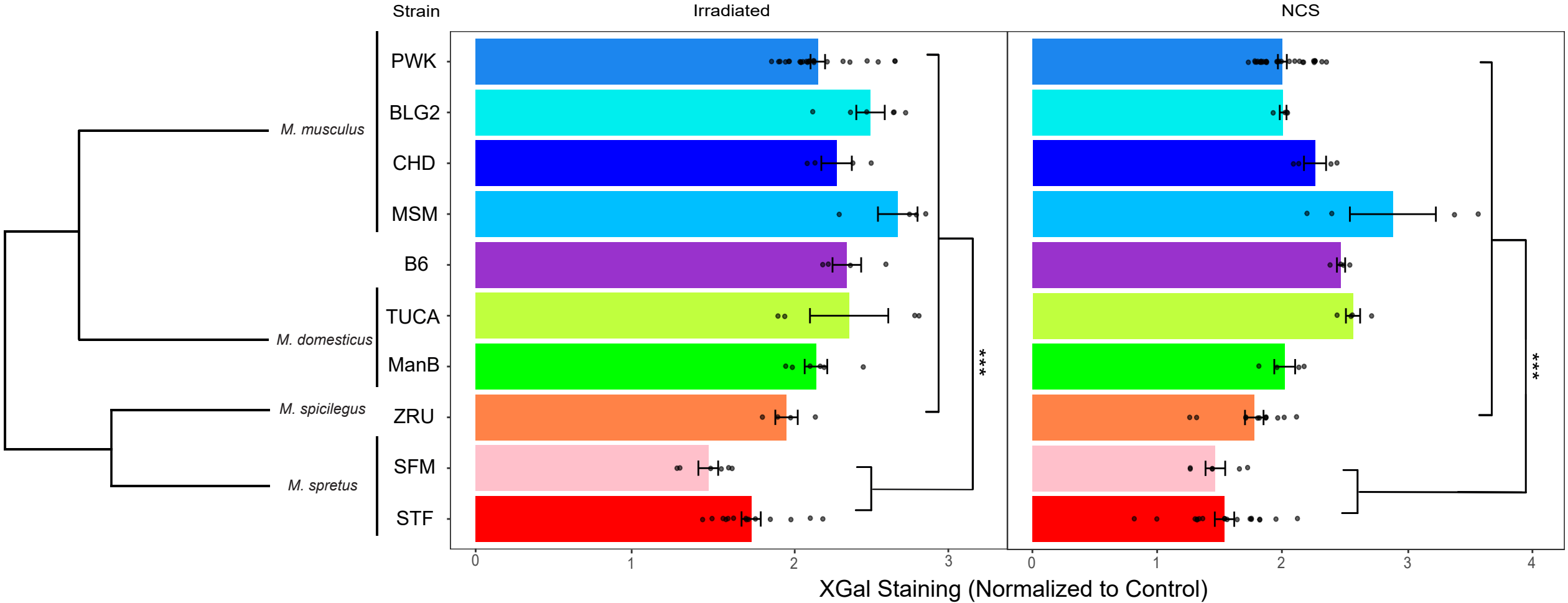
Strain
Irradiated
NCS
PWK
BLG2
CHD
MSM
B6
TUCA
ManB
ZRU
SFM
STF
M. musculus
M. domesticus
M. spicilegus
M. spretus
***
***
0
1
2
3
0
1
2
3
4
XGal Staining (Normalized to Control)

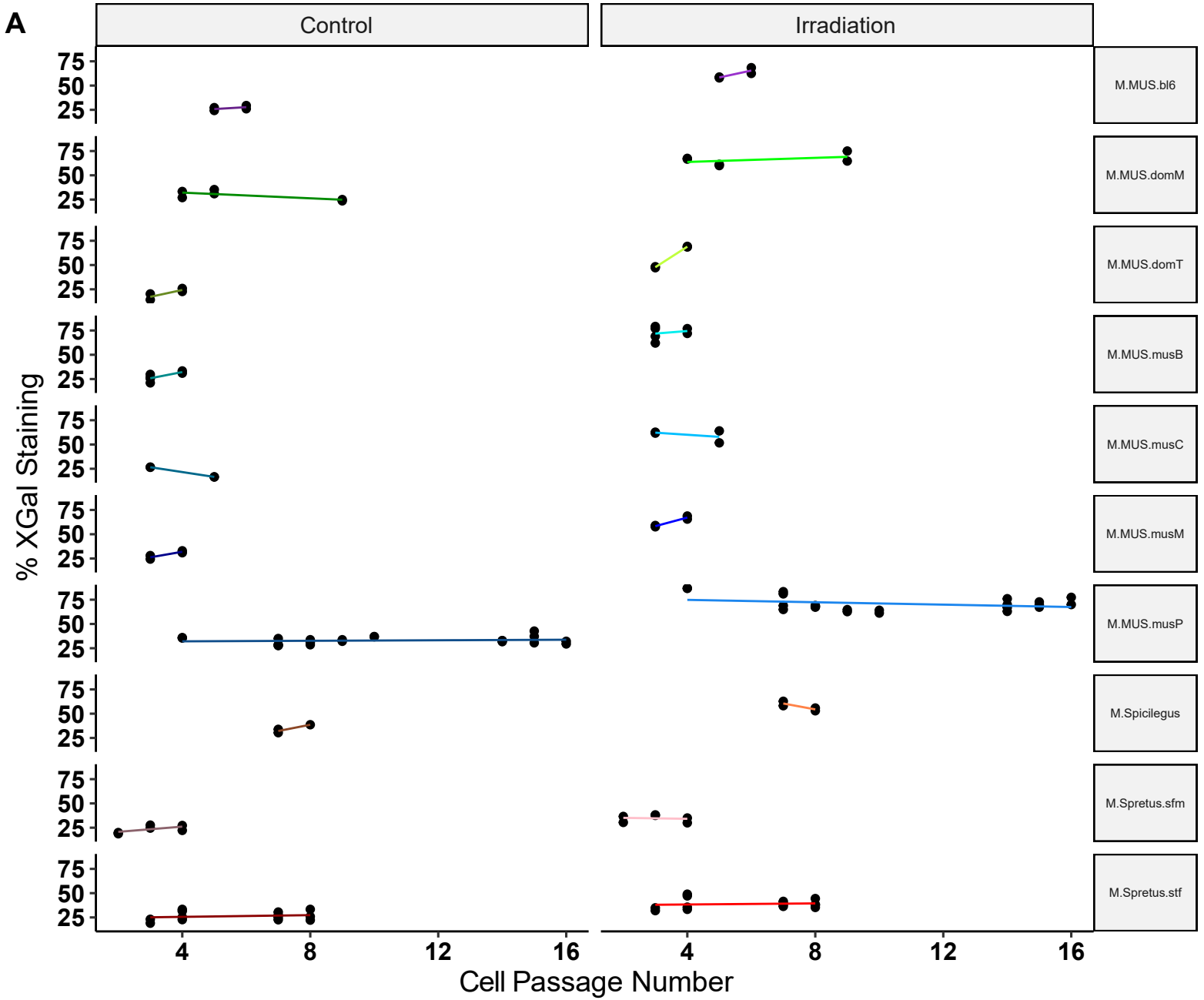
A
Control
Irradiation
M.MUS.bl6
M.MUS.domM
M.MUS.domT
M.MUS.musB
M.MUS.musC
M.MUS.musM
M.MUS.musP
M.Spicilegus
M.Spretus.sfm
M.Spretus.stf
% XGal Staining
75
50
25
4
8
12
16
Cell Passage Number

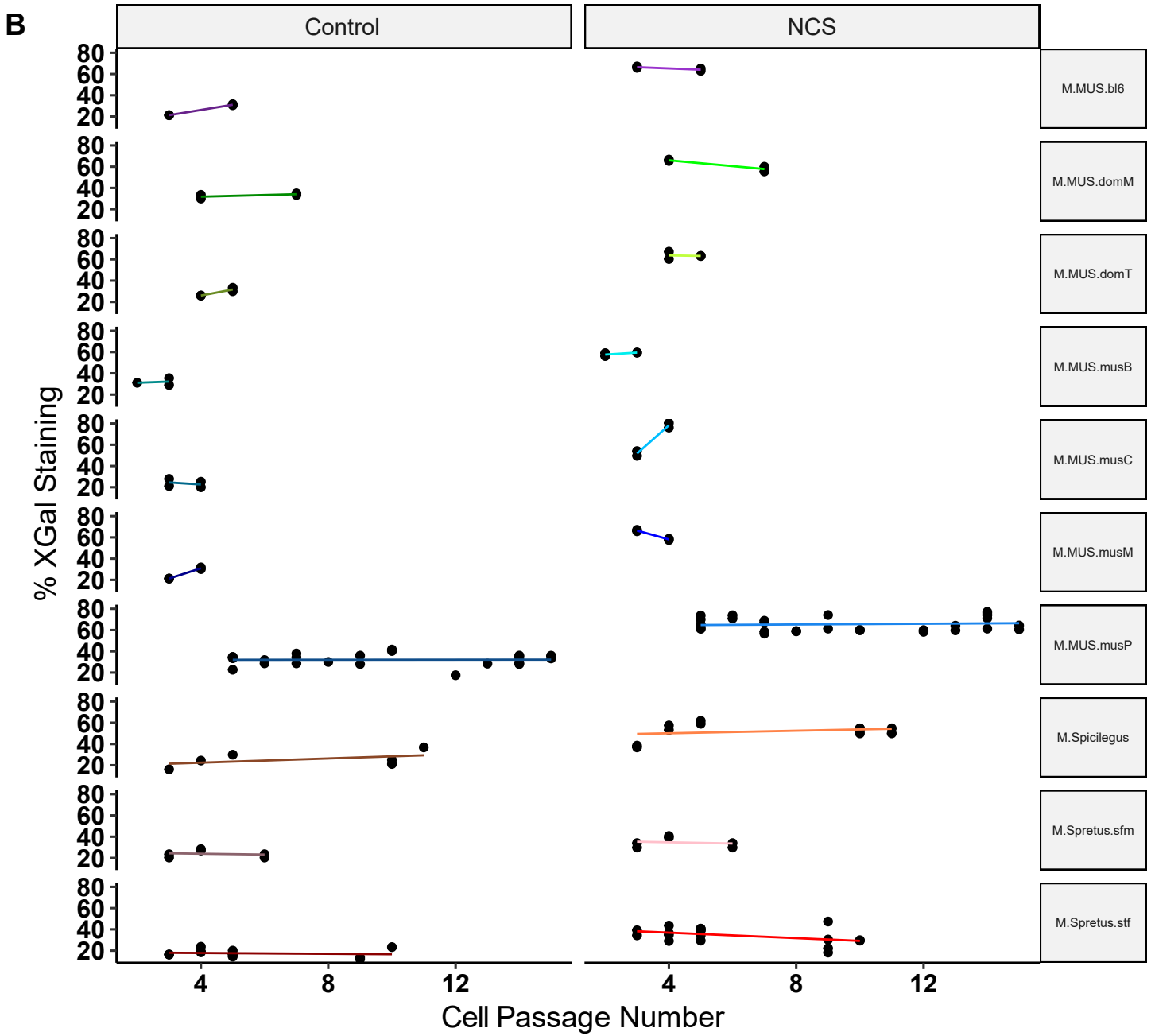
B
Control
NCS
M.MUS.bl6
M.MUS.domM
M.MUS.domT
M.MUS.musB
M.MUS.musC
M.MUS.musM
M.MUS.musP
M.Spicilegus
M.Spretus.sfm
M.Spretus.stf
% XGal Staining
Cell Passage Number
80
60
40
20
4
8
12

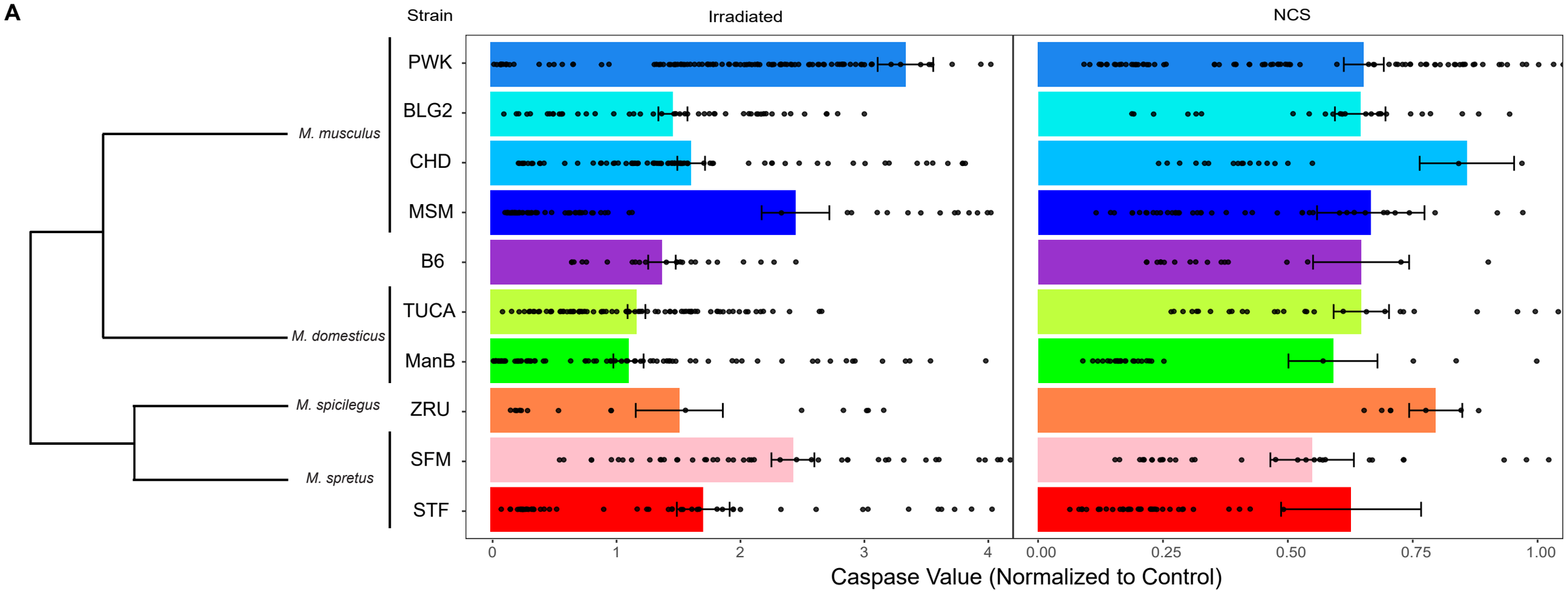
A
Strain
Irradiated
NCS
PWK
BLG2
CHD
MSM
B6
TUCA
ManB
ZRU
SFM
STF
M. musculus
M. domesticus
M. spicilegus
M. spretus
0
1
2
3
4
0.00
0.25
0.50
0.75
1.00
Caspase Value (Normalized to Control)

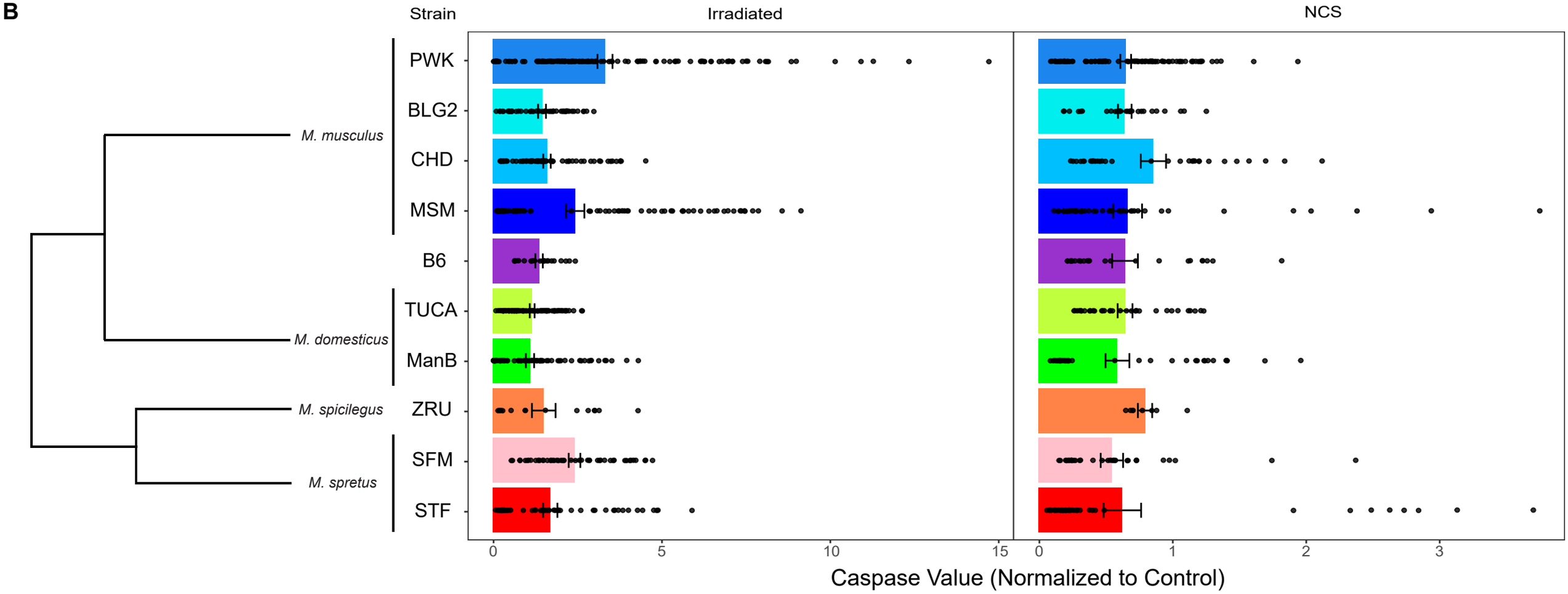
B
Strain
Irradiated
NCS
PWK
BLG2
CHD
MSM
B6
TUCA
ManB
ZRU
SFM
STF
M. musculus
M. domesticus
M. spicilegus
M. spretus
0
5
10
15
0
1
2
3
Caspase Value (Normalized to Control)

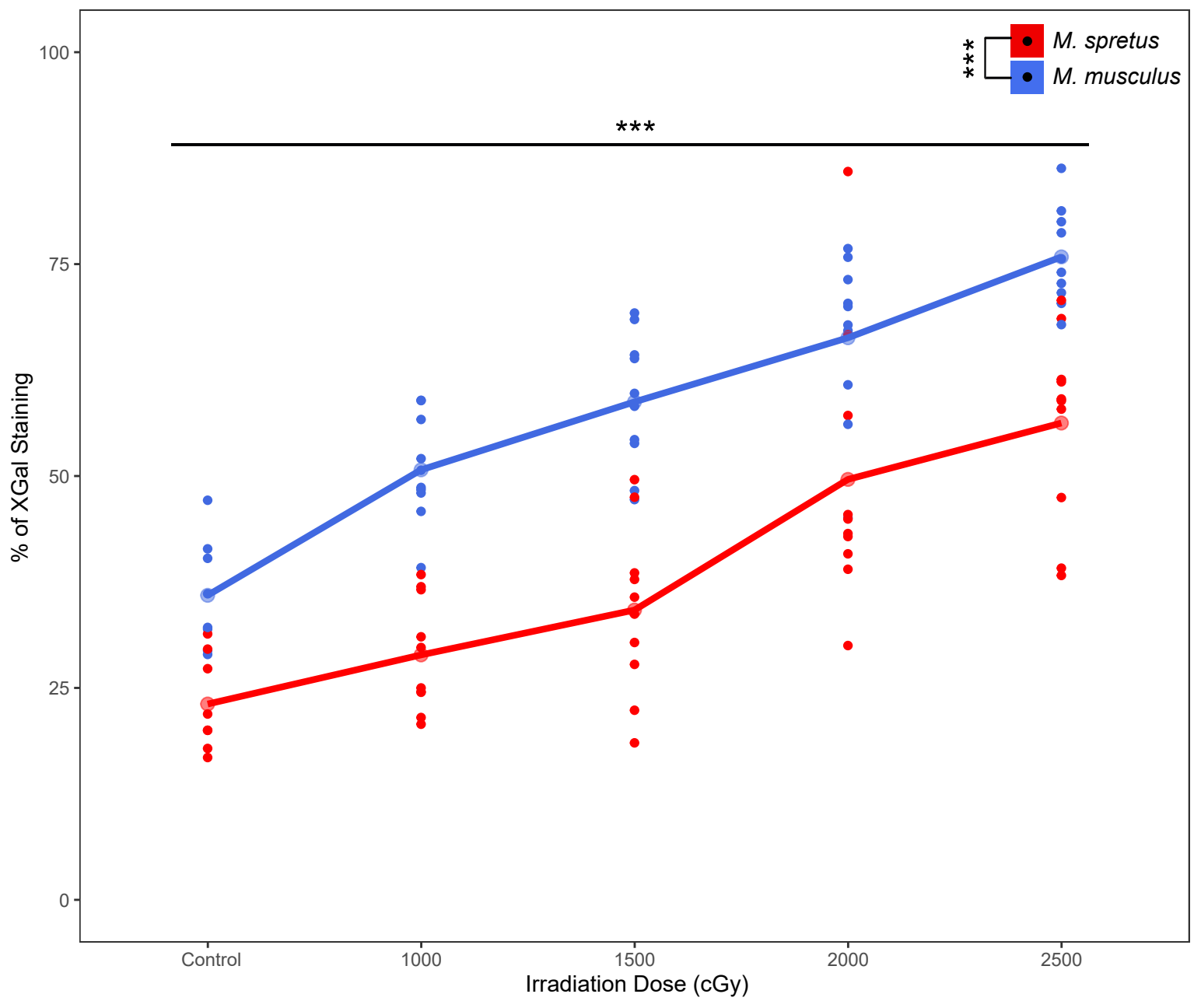
M. spretus
M. musculus
***
***
100
75
50
25
0
% of XGal Staining
Control
1000
1500
2000
2500
Irradiation Dose (cGy)

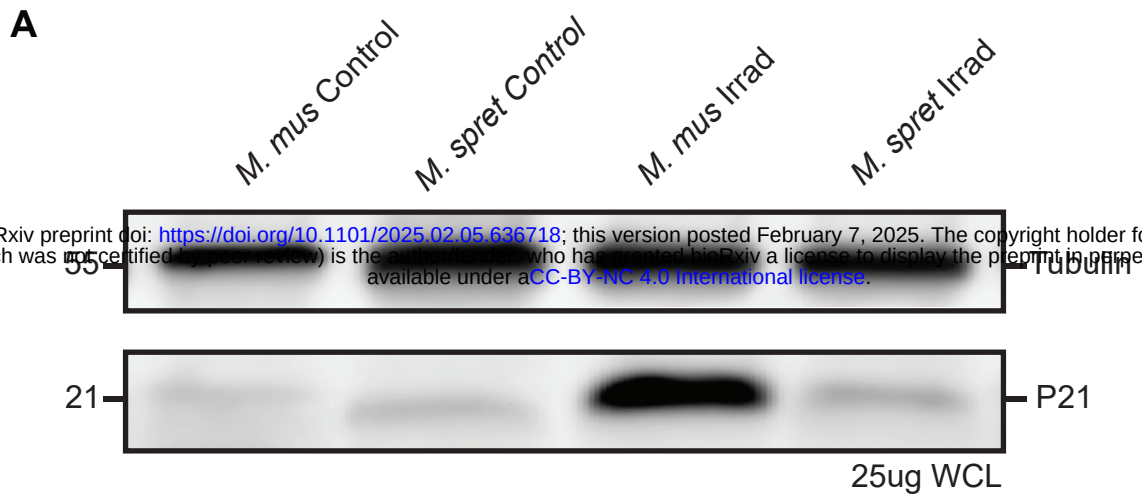

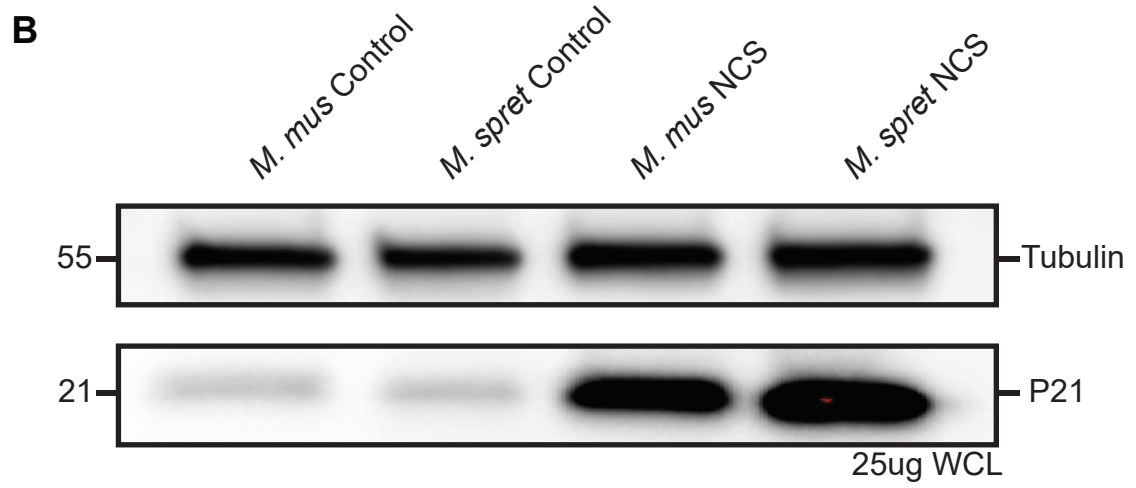

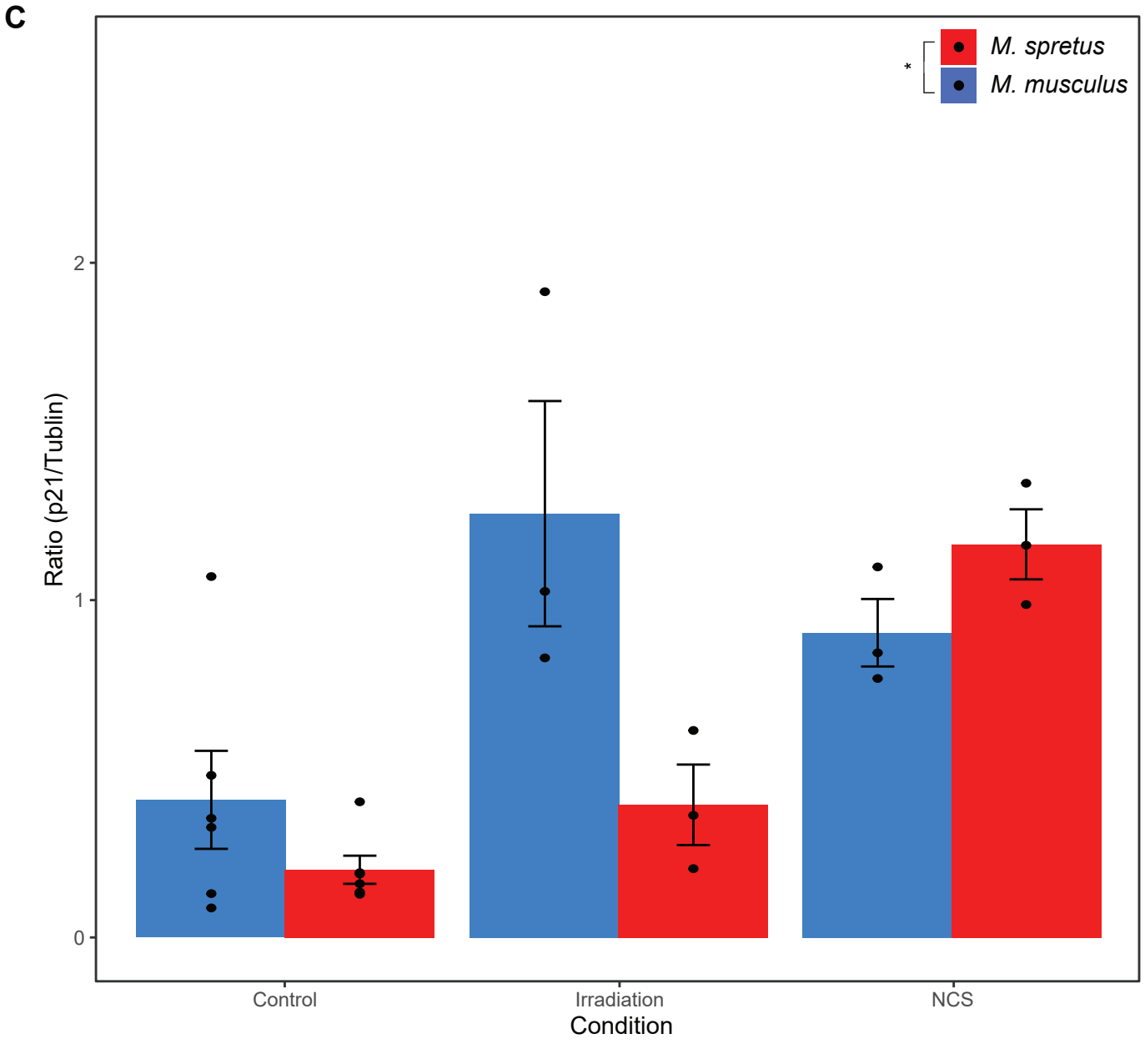

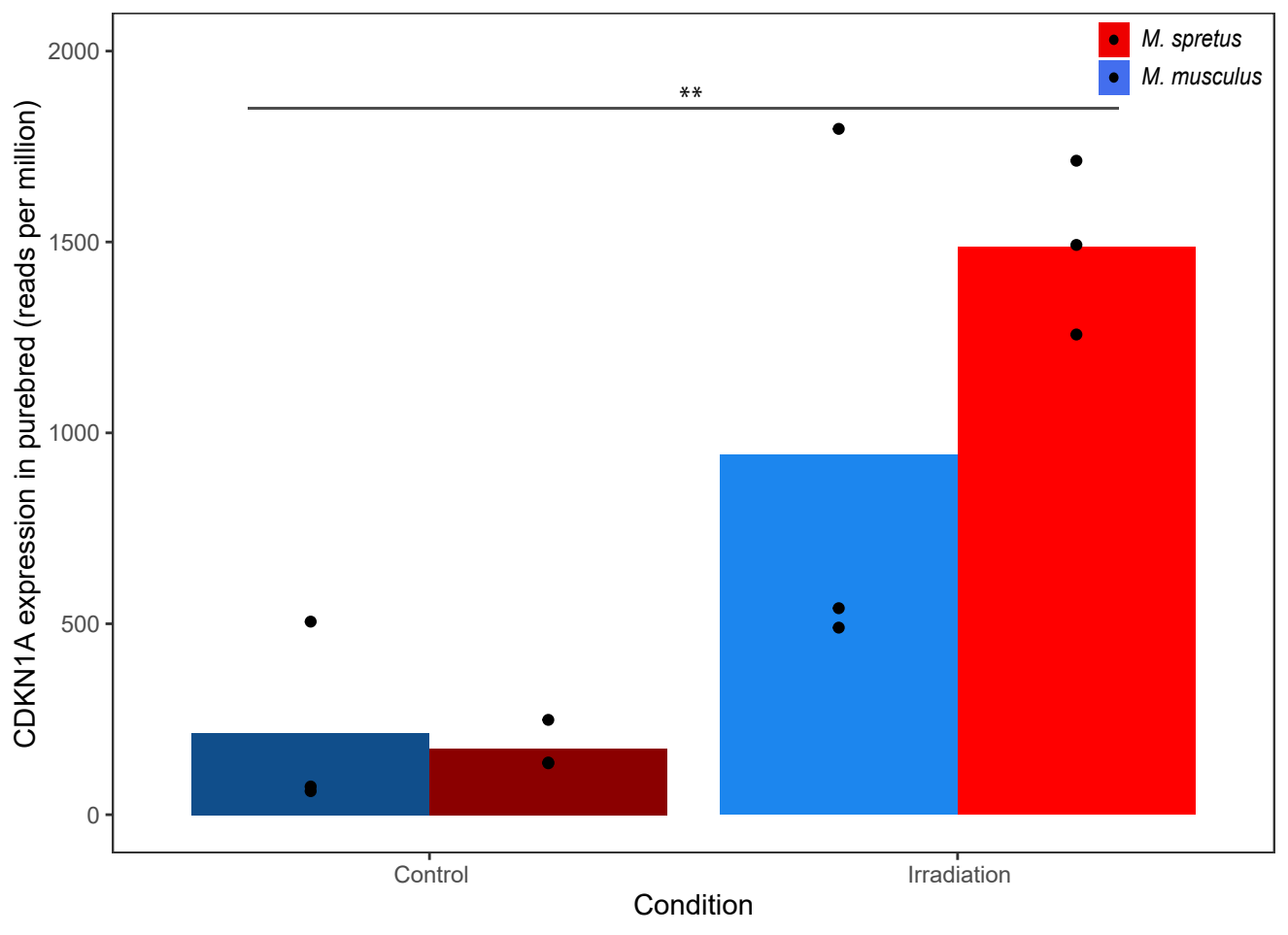
M. spretus
M. musculus
**
2000
1500
1000
500
0
CDKN1A expression in purebred (reads per million)
Control
Irradiation
Condition

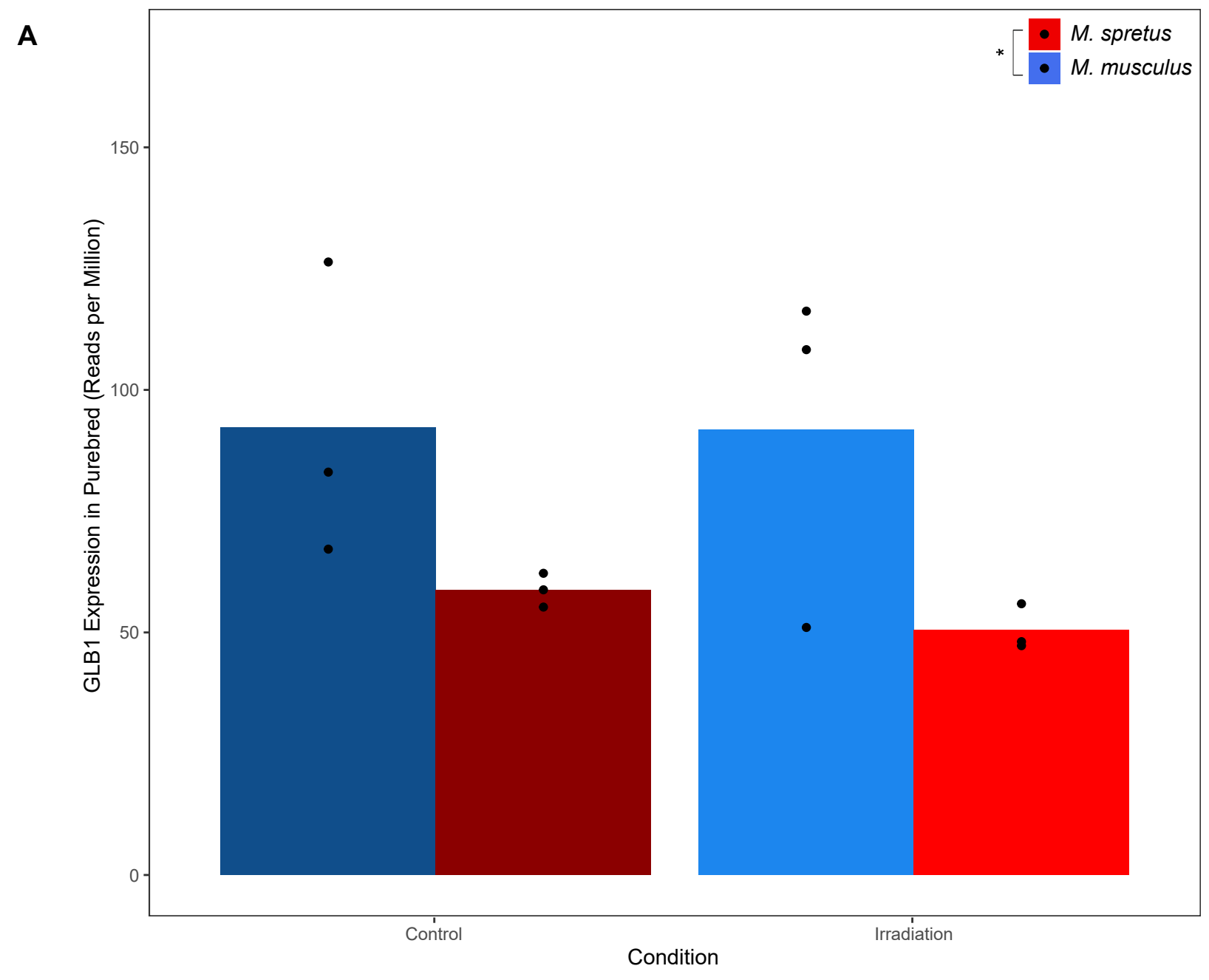
A
M. spretus
M. musculus
*
150
100
50
0
GLB1 Expression in Purebred (Reads per Million)
Control
Irradiation
Condition

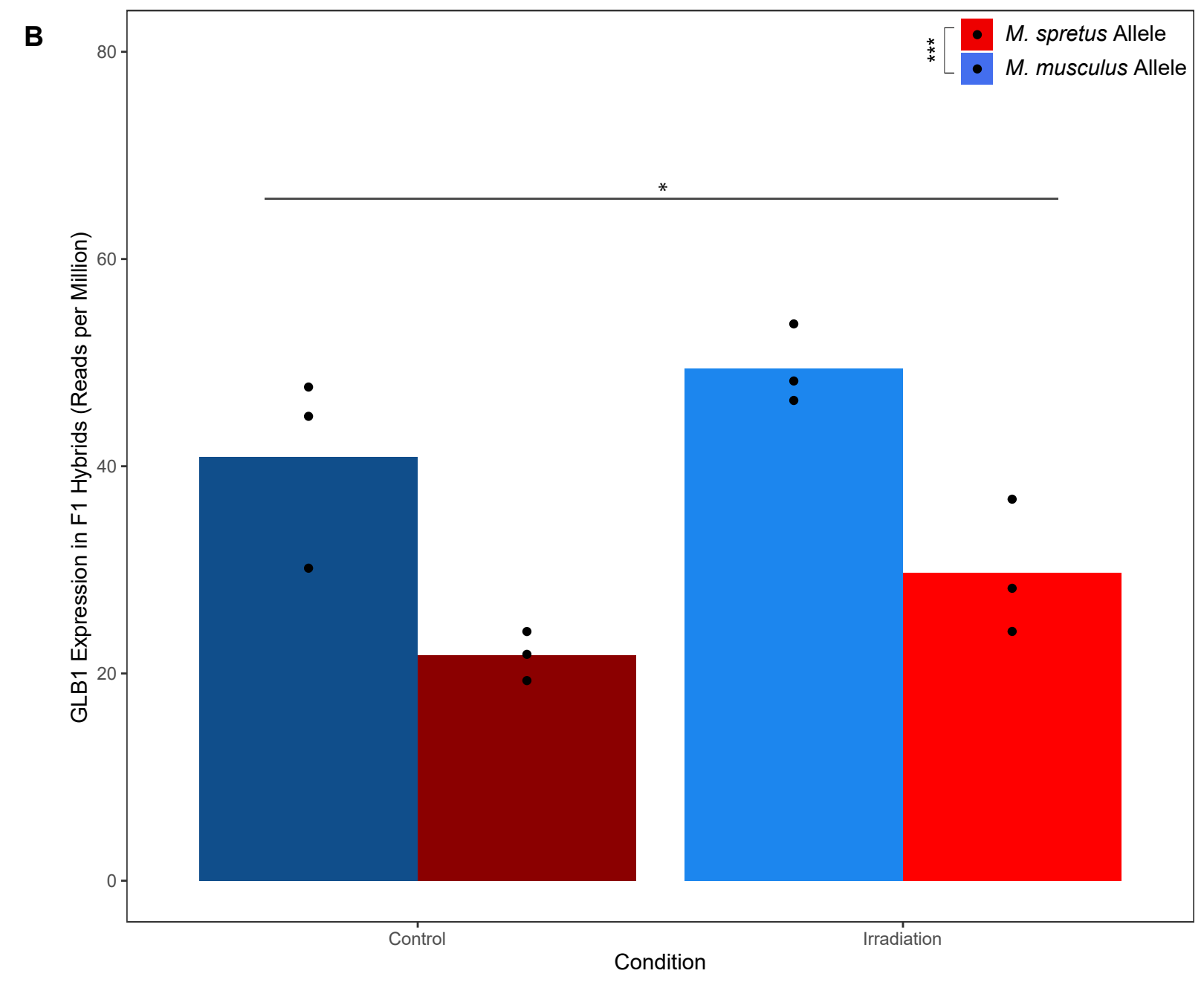
B
80
60
40
20
0
GLB1 Expression in F1 Hybrids (Reads per Million)
M. spretus Allele
M. musculus Allele
***
*
Control
Irradiation
Condition